Acoustic diffraction from the junction of two joined parallel plates

Andrew N. Norris
Department of Mechanical and Aerospace Engineering, Rutgers University, Piscataway, New Jersey 08855-0909

(Received 4 August 1995; accepted for publication 13 November 1995)

Two parallel semi-infinite plates are joined together at their common end, with vacuum in the infinitesimal gap between them and acoustic fluid outside. The configuration is an idealization of a realistic structural member such as the bow or keel of a ship where the structural elements are joined at an acute angle. The exact solution for acoustic diffraction from the parallel double plate junction is obtained using thin plate theory and the Wiener–Hopf technique. The diffraction coefficient is strongly dependent upon frequency, unlike the analogous coefficients for edge diffraction from hard or soft screens. However, the relative simplicity of the general solution permits analytical comparisons with these idealized boundary conditions. At low frequencies the diffraction simulates the response from a soft or pressure release screen. At high frequencies, or more precisely under light fluid-loading conditions, the hard screen approximation is more appropriate. Numerical examples illustrate the transition from soft to hard diffraction, and an approximate but simple uniform diffraction coefficient is proposed which has the correct limiting behavior at low and high frequency.

PACS numbers: 43.40.Dx, 43.40.Rj

INTRODUCTION

The structural element depicted in Fig. 1 is typical of bows and keels on ships and large ocean going vessels. It is composed of two similar plate or shell segments that meet along a line, where they are structurally attached in the sense that forces and bending moments may be transmitted from one to the other, but only along the join. The purpose of this paper is to examine the interaction and diffraction of an incident acoustic sound wave, as shown in Fig. 1. We will concentrate on the acoustic-to-acoustic diffraction emanating from the vertex, and in particular, we restrict attention to acute structural angles such that the bow junction is approximated for convenience as a double plate junction, as depicted in Fig. 2.

This type of structural acoustics problem is prototypical of bow-type configurations, and an understanding of it is fundamental to interpreting first arrival diffracted acoustic waves. Thus one might ask whether the double plate junction is acoustically more akin to either a hard (or rigid) screen in the same position, or a screen with pressure release boundary conditions—a "soft" screen. Edge diffraction from these limiting structures is well understood, and the associated diffraction coefficients have simple forms.[1] In particular, the hard and soft acoustic diffraction coefficients are independent of frequency. The response from the double plates is expected to depend strongly on frequency, but as we will see, it behaves like the soft and hard screens at low and high frequencies, respectively.

Despite the ubiquity of the double plate configuration and its acoustic significance, it does not appear that this acoustic diffraction problem has been considered until now. Thus Crighton's review article[2] mentions many related but different problems. The most relevant of these is the case of a *single* plate in the position of the double plate structure of Fig. 2. However, despite the apparent similarity, the acoustical behavior of the single plate and double plates are quite distinct, as we will show later. In particular, the single plate solution does not suffice for the double plate, but the single plate solution is contained within the latter. The present diffraction problem is, however, mathematically similar to that for the single plate in that we need to use the Wiener–Hopf technique to derive the pressure transform. Diffraction from a single plate was first analyzed by Lamb,[3] and Lyamshev[4] subsequently included the effects of flow, but both papers treat the light fluiding limit only, and they suffer from a fundamental error in the Wiener–Hopf analysis.[5] The correct solution was provided by Cannell, who in a series of two papers,[6,7] gave a detailed account of the proper procedure for solving the problem posed by Lamb, although Cannell's solution is limited in its applicability, as we discuss below. The present analysis is also related to Wiener–Hopf solutions for structural elements composed of flat plates joined end to end,[8–13] although such configurations are quite distinct from the present one. However, we will draw upon some recent results[11] in this area to derive very explicit and simple formulae for the diffraction coefficient.

The exact problem and the general method of its solution are outlined in Sec. I. The analytical details of the Wiener–Hopf method are discussed in Sec. II, followed by a general discussion of the acoustic diffraction coefficient in Sec. III. There we examine the relationship between the general exact solution and the simpler limiting diffraction coefficients for soft and hard screens.

I. FORMULATION OF THE SCATTERING PROBLEM

A. Dynamic equations

We consider time harmonic motion of frequency $\omega > 0$, the factor $\mathrm{Re}\{\cdot e^{-i\omega t}\}$ understood but suppressed. We restrict

 0001-4966/96/99(3)/1475/9/$6.00

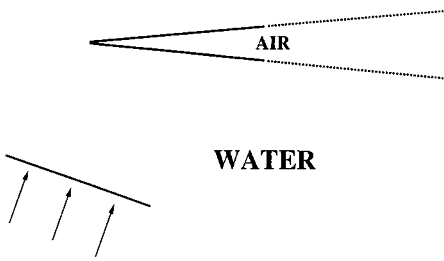

FIG. 1. A plane acoustic wave incident on the bow of a ship.

the analysis to the two-dimensional configuration, see Fig. 2, where the plates lie along the positive x axis. The acoustic pressure $p(x,y)$ satisfies the Helmholtz equation in the fluid region,

$$\nabla^2 p+k^2 p=0, \quad -\infty<x<\infty, \quad -\infty<y<\infty, \tag{1}$$

where $k=\omega/c$ is the acoustic wave number and c is the fluid sound speed. The plate deflection in the positive y direction on the top and bottom plates are $w_\pm(x)$, respectively. The equation of kinematic continuity between the plates and the fluid is

$$\rho\omega^2 w_\pm(x)=\frac{\partial p}{\partial y}(x,\pm 0), \quad 0<x<\infty, \tag{2}$$

where ρ is the fluid mass density. The two plates are identical and are modeled by the classical theory of dynamic flexure,

$$B\,\frac{d^4 w_\pm}{dx^4}(x)-m\omega^2 w_\pm(x)=\mp p(x,\pm 0), \quad 0<x<\infty. \tag{3}$$

The plate parameters are the mass per unit area m and the bending stiffness B and are constant on each plate. These quantities may be related to the intrinsic plate properties; thus $m=\rho_s h$, and $B=Eh^3/12(1-\nu^2)$, where h, ρ_s, E, and ν are the thickness, volumetric mass density, Young's modulus, and Poisson ratio, respectively. We note that the acoustic pressure in the infinitesimal gap between the plates is assumed to be zero. Thus the only interaction between the plates is through the fluid and the junction.

Eliminating the plate deflection between the pair of boundary conditions in Eqs. (2) and (3) reduces them to a single equation for the pressure,

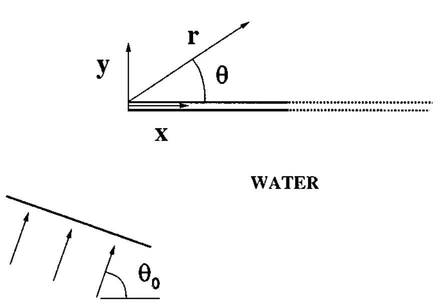

FIG. 2. The idealized junction formed from two parallel elastic plates joined at the end.

$$\left(B\,\frac{\partial^4}{\partial x^4}-m\omega^2\right)\frac{\partial p}{\partial y}\pm\rho\omega^2 p=0, \quad 0<x<\infty, \quad y=\pm 0. \tag{4}$$

The diffraction problem can now be formulated entirely in terms of the pressure. Thus we need to solve the Helmholtz equation (1) in the fluid, subject to radiation conditions as $(x^2+y^2)^{1/2}\to\infty$ and the boundary conditions (4) on $y=\pm 0$. Four edge conditions must be specified at the junction $x=y=0$. The plates are assumed to be in contact only at $x=0$ with no interaction for $x>0$. The ends at $x=0$ are mechanically joined such that the displacements and rotations are identical there, and the moments and shear forces on either plate are equal and opposite. The moment and force conditions ensure that the tip has zero net moment and force acting, but there are still non zero moments and forces between the plates. Thus

$$w_+(0)=w_-(0), \tag{5a}$$

$$\frac{dw_+}{dx}(0)=\frac{dw_-}{dx}(0), \tag{5b}$$

$$B\,\frac{d^2 w_+}{dx^2}(0)=-B\,\frac{d^2 w_-}{dx^2}(0), \tag{5c}$$

$$B\,\frac{d^3 w_+}{dx^3}(0)=-B\,\frac{d^3 w_-}{dx^3}(0). \tag{5d}$$

The formulation of the problem is complete once we have specified the incident wave field, $p^{(0)}$, which we take to be a plane wave,

$$p^{(0)}(x,y)=p_0 e^{ik(x\cos\theta_0+y\sin\theta_0)}. \tag{6}$$

B. Solution procedure

We split the total pressure into two parts,

$$p(x,y)=p_S(x,y)+p_A(x,y), \tag{7}$$

such that p_S and p_A are, respectively, symmetric and antisymmetric about the line $y=0$, that is,

$$\begin{aligned} p_S(x,y)&=(p(x,y)+p(x,-y))/2,\\ p_A(x,y)&=(p(x,y)-p(x,-y))/2. \end{aligned} \tag{8}$$

For each constituent we need only consider the problem defined in $y\geqslant 0$. Thus for the symmetric part of the pressure the conditions on $y=0$ are

$$\frac{\partial p_S}{\partial y}=0, \quad -\infty<x<0, \quad y=0, \tag{9a}$$

$$\left(B\,\frac{\partial^4}{\partial x^4}-m\omega^2\right)\frac{\partial p_S}{\partial y}+\rho\omega^2 p_S=0, \quad 0<x<\infty, \quad y=0. \tag{9b}$$

The antisymmetric part of the pressure satisfies

$$p_A=0, \quad -\infty<x<0, \quad y=0, \tag{10a}$$

$$\left(B\,\frac{\partial^4}{\partial x^4}-m\omega^2\right)\frac{\partial p_A}{\partial y}+\rho\omega^2 p_A=0, \quad 0<x<\infty, \quad y=0. \tag{10b}$$

The end conditions can be found by noting that $w_{\pm}(x)=w_S(x)\pm w_A(x)$, where

$$\rho\omega^2 w_S(x)=\frac{\partial p_S}{\partial y}(x,+0), \quad \rho\omega^2 w_A(x)=\frac{\partial p_A}{\partial y}(x,+0). \tag{11}$$

The conditions (5a) and (5b) therefore become

$$w_S(0)=0, \quad \frac{dw_S}{dx}(0)=0, \tag{12}$$

while (5c) and (5d) are

$$\frac{d^2w_A}{dx^2}(0)=0, \quad \frac{d^3w_A}{dx^3}(0)=0. \tag{13}$$

The procedure for finding the separate solutions of different parity is similar. In either case we let

$$p_\alpha(x,y)=p_\alpha^{(0)}(x,y)+p_\alpha^{(1)}(x,y), \quad \alpha=S \text{ or } A, \tag{14}$$

where $p_S^{(0)}$ and $p_A^{(0)}$ are the symmetric and antisymmetric parts of the incident field, while $p_S^{(1)}$ and $p_A^{(1)}$ are the symmetric and antisymmetric parts of the scattered pressure. The latter automatically satisfy the Helmholtz equation (1) if we write them as

$$p_\alpha^{(1)}(x,y)=\frac{1}{2\pi}\int_{-\infty}^{\infty}\tilde{p}_\alpha(\xi)e^{(i\xi x-\gamma(\xi)y)}\,d\xi,$$
$$-\infty<x<\infty, \quad 0\leqslant y<\infty, \tag{15}$$

for $\alpha=S$ or $\alpha=A$. The square root function $\gamma(\xi)=(\xi^2-k^2)^{1/2}$ is defined to be analytic in the complex ξ plane with two L-shaped branch cuts from $-k$ to $-i0$ to $-i\infty$, and from k to $i0$ to $i\infty$, such that the real part of γ is non-negative. For convenience, we have given k a small positive imaginary part, i.e., $k=|k|e^{i\delta_1}$, $0<\delta_1\ll 1$. Along the real axis $\gamma(\xi)=-i\sqrt{k^2-\xi^2}$ for $|\xi|<|k|$ and $\gamma(\xi)=\sqrt{\xi^2-k^2}$ for $|\xi|>|k|$. The difficulty is now reduced to finding the transforms $\tilde{p}_S$ and $\tilde{p}_A$, which we address separately for the two subproblems.

C. Physical significance of the two problems

The separate problems for p_S and p_A can each be related to the acoustic scattering from a single plate in a fluid medium. Thus the symmetric pressure $p_S(x,y)$ for $y>0$ corresponds to the solution for a plate joined to an infinite baffle. That is, the semi-line $x<0$, $y=0$ is a rigid baffle, and the point at which the plate meets the baffle is pinned (or clamped). We note that Cannell[7] considered a similar plate and baffle configuration but with the plate end free of moment and shear force.

The antisymmetric solution, p_A, is simply the antisymmetric part of the total pressure field for the plane wave $p^{(0)}$ incident on a plate with bending stiffness $B'=2B$ and mass density $m'=2m$ in an infinite fluid medium, and which is free of moment and shear at its end. In order to see this we note that the antisymmetric pressure p_A on the double plate system of Fig. 2 bends both plates in the same direction, so that $w_+=w_-$. The pressure drop from one side to the other is $2p_A$, but the pressure drop acting on each plate is just p_A because it is assumed that the acoustic pressure is identically zero in the infinitesimal unflooded gap between them, and hence the governing equation (10b). However, the pressure drop across a *single* plate in a fluid is $2p_A$, and its equation is therefore

$$\left(B'\frac{\partial^4}{\partial x^4}-m'\omega^2\right)\frac{\partial p_A}{\partial y}+2\rho\omega^2 p_A=0, \quad 0<x<\infty, \quad y=0, \tag{16}$$

with the same end conditions as Eq. (13). A comparison of Eqs. (10b) and (16) shows that the antisymmetric parts of the pressure for the double plate and single plate problems are the same if the single plate has bending stiffness and mass per unit length that are both twice the values for the individual plates in the original problem. Another way of looking at it is that the double plate system has an effective bending stiffness of $2B$ and its effective mass density is $2m$.

As mentioned in the Introduction, acoustic diffraction from a single plate has been considered in detail by Cannell.[6,7] The problem can be reduced to a Wiener–Hopf analysis for the half-space $-\infty<x<\infty$, $0\leqslant y<\infty$ with different conditions along the boundary $y=0$ on the half-lines $-\infty<x<0$, and $0<x<\infty$. In his first paper Cannell[6] derived the full formal solution,[14] but only analyzed the limiting case of light fluid loading. The general results for arbitrary fluid loading were given in an indirect form involving two unknown parameters, p and q, which must be obtained by solving four simultaneous equations. In the second paper,[7] Cannell examined the heavy fluid-loading limit, but for a *different* problem in which there is a baffle present on the half-line complementary to the plate, although the plate is still free at $x=y=0$ (no moment or shear force act). The diffraction from the end of the baffle turns out to dominate the acoustic diffraction in the far field, leaving open the question of the precise form of the acoustic diffraction from an *isolated plate edge* in the heavy fluiding-loading regime. We will answer this in Sec. III. In summary, the problem considered here concerns the double plate geometry of Fig. 2, but the antisymmetric part of the full solution is closely related to the single plate problem. In fact, we will obtain a very explicit formula for the double plate solution from which we can easily extract the response for the single plate in a fluid.

II. WIENER–HOPF ANALYSIS

A. Solution of the symmetric problem

Substituting the assumed form of the solution, defined by Eq. (14) and the transform of Eq. (15), into the two boundary conditions of Eq. (9a) and (9b) and using Eq. (6), yields two simultaneous integral equations for the unknown $\tilde{p}_S(\xi)$,

$$\frac{1}{2\pi}\int_{-\infty}^{\infty}\gamma(\xi)\tilde{p}_S(\xi)e^{i\xi x}\,d\xi=0, \quad x<0, \tag{17a}$$

$$\frac{1}{2\pi}\int_{-\infty}^{\infty}D(\xi)\tilde{p}_S(\xi)e^{i\xi x}\,d\xi=-A_S^{(0)}D(\xi_0)e^{i\xi_0 x}, \quad x>0, \tag{17b}$$

where $\xi_0 = k\cos\theta_0$, $A_S^{(0)} = (D(\xi_0))^{-1} p_0$, and D is the fluid-loaded plate dispersion function,

$$D(\xi) = 1 + (m\omega^2 - B\xi^4)\gamma(\xi)/(\rho\omega^2). \tag{18}$$

Dual integral equations like these can be solved using the Wiener–Hopf technique.[15] We will not go into the details of the method, but just provide a solution which will be shown to satisfy the integral equations. Let

$$K(\xi) = D(\xi)/\gamma(\xi), \tag{19}$$

and define $K^{\pm}(\xi)$ as Wiener–Hopf factors such that

$$K(\xi) = K^+(\xi)/K^-(\xi) \quad \text{with} \quad K^-(-\xi) = 1/K^+(\xi). \tag{20}$$

The functions $K^{\pm}(\xi)$ are analytic in the half-planes $\mathscr{H}^{\pm}$, where $\mathscr{H}^{\pm}$ are the upper and lower half-planes, $\text{Im}\ \xi \gtrless \mp\delta_2$, where $0 < \delta_2 \leqslant 1$ is related to δ_1 and is included to ensure a small region of overlap that includes the real axis.[15] The general solution for the pressure transform is

$$\tilde{p}_S(\xi) = \frac{iA_S(\xi)}{\xi - \xi_0} \frac{G_S(\xi_0)}{G_S(\xi)}, \tag{21}$$

where G_S is

$$G_S(\xi) \equiv D(\xi)/K^+(\xi) = \gamma(\xi)/K^-(\xi), \tag{22}$$

and $A_S(\xi)$ is a polynomial of as yet unspecified degree q, $q \geqslant 0$, satisfying

$$A_S(\xi_0) = A_S^{(0)}. \tag{23}$$

It can be shown by direct substitution of $\tilde{p}_S$ from Eq. (21) into the two integral equation (17a) and (17b) that they are automatically satisfied. Thus, the left member of Eq. (17a) becomes, using the second identity of Eq. (22),

$$\frac{G_S(\xi_0)}{2\pi i} \int_{-\infty}^{\infty} \frac{K^-(\xi)}{\xi_0 - \xi} e^{i\xi x}\, d\xi. \tag{24}$$

If $x < 0$ then the integrand is clearly analytic in $\mathscr{H}^-$, and the contour can be deformed to one at infinity in the same half-plane, along which the integrand is zero, implying that the integral vanishes for *any* function $K^-(\xi)$ that is analytic in $\mathscr{H}^-$ with appropriate behavior at infinity. Similarly, using the first identity of Eq. (22) it follows that Eq. (17b) holds for any $K^+(\xi)$ analytic in $\mathscr{H}^+$. The arbitrariness in the choice of $K^{\pm}(\xi)$ is removed by the restriction from Eq. (22) that $D/K^+ = \gamma/K^-$. However, the general solution still contains an undetermined polynomial $A_S(\xi)$. The problem therefore consists of (i) factorizing K and (ii) finding the polynomial $A_S(\xi)$. The first of these is outlined in the Appendix, so we will proceed to the determination of A_S.

First we note that the deflection for the symmetric solution can be expressed as

$$\rho\omega^2 w_S(x) = \frac{\partial p_S^{(0)}}{\partial y}(x,0) - A_S\left(-i\frac{d}{dx}\right) W_S(x), \tag{25}$$

where

$$W_S(x) = \frac{1}{2\pi i} \int_{-\infty}^{\infty} \tilde{W}_S(\xi) e^{i\xi x}\, d\xi, \tag{26a}$$

$$\tilde{W}_S(\xi) = \frac{-\gamma(\xi)}{\xi - \xi_0} \frac{G_S(\xi_0)}{G_S(\xi)}. \tag{26b}$$

Using Eqs. (19), (20), and (22), we have

$$\tilde{W}_S(\xi) = -G_S(\xi_0) \frac{K^-(\xi)}{\xi - \xi_0}, \tag{27}$$

which is analytic in $\mathscr{H}^-$. Furthermore, it follows from Eqs. (18) through (20) that $K^-(\xi) = O(\xi^{-2})$ as $|\xi| \to \infty$, and hence $\tilde{W}_S(\xi) = O(\xi^{-3})$ in the same limit. The inverse transform $W_S(x)$ consequently has leading-order behavior like $W_S(x) = O(x^2)$ for $x \to +0$, and therefore the end conditions of Eq. (12) are automatically satisfied if the polynomial $A_S(\xi)$ is simply a constant $(q = 0)$. Hence, using Eq. (23),

$$A_S(\xi) = A_S^{(0)}. \tag{28}$$

This completes the solution to the symmetric problem.

B. Solution of the antisymmetric problem

Dual integral equations for the transform $\tilde{p}_A$ follow from Eqs. (6), (10a), (10b), and (15),

$$\frac{1}{2\pi} \int_{-\infty}^{\infty} \tilde{p}_A(\xi) e^{i\xi x}\, d\xi = 0, \quad x < 0, \tag{29a}$$

$$\frac{1}{2\pi} \int_{-\infty}^{\infty} D(\xi)\tilde{p}_A(\xi) e^{i\xi x}\, d\xi = -A_A^{(0)} D(\xi_0) e^{i\xi_0 x}, \quad x > 0, \tag{29b}$$

where $A_A^{(0)} = [1 - (D(\xi_0))^{-1}] p_0$. The general solution is

$$\tilde{p}_A(\xi) = \frac{iA_A(\xi)}{\xi - \xi_0} \frac{G_A(\xi_0)}{G_A(\xi)}, \tag{30}$$

where G_A is

$$G_A(\xi) \equiv D(\xi)/D^+(\xi) = 1/D^-(\xi), \tag{31}$$

and $A_A(\xi)$ is a polynomial satisfying

$$A_A(\xi_0) = A_A^{(0)}. \tag{32}$$

The Wiener–Hopf factors $D^{\pm}(\xi)$ are analytic in the half-planes $\mathscr{H}^{\pm}$ and satisfy

$$D(\xi) = D^+(\xi)/D^-(\xi) \quad \text{with} \quad D^-(-\xi) = 1/D^+(\xi). \tag{33}$$

The factorization is closely related to the factorization for the symmetric problem and is discussed in detail in the Appendix.

The deflection for the antisymmetric solution can be written in the same form as the symmetric solution in Eq. (25), but now using the function W_A and its transform $\tilde{W}_A(\xi)$. Thus

$$\rho\omega^2 w_A(x) = \frac{\partial p_A^{(0)}}{\partial y}(x,0) - A_A\left(-i\frac{d}{dx}\right) W_A(x), \tag{34a}$$

$$W_A(x) = \frac{1}{2\pi i} \int_{-\infty}^{\infty} \tilde{W}_A(\xi) e^{i\xi x}\, d\xi, \tag{34b}$$

where

$$\tilde{W}_A(\xi)=\frac{-\gamma(\xi)}{\xi-\xi_0}\frac{G_A(\xi_0)}{G_A(\xi)}. \tag{35}$$

The functions $\tilde{W}_A^-(\xi)$ and $\tilde{W}_A^+(\xi)$ are defined to be analytic in $\mathscr{H}^\pm$, respectively, and they partition $\tilde{W}_A$ as

$$\tilde{W}_A(\xi)=\tilde{W}_A^+(\xi)+\tilde{W}_A^-(\xi), \tag{36}$$

and both $\tilde{W}_A^\pm=O(\xi^{-1})$ as $|\xi|\to\infty$. The behavior of $W_A(x)$ for $x\to+0$, and hence the response near the end, depends upon the behavior of $\tilde{W}_A^-(\xi)$ as $|\xi|\to\infty$.

The transform $\tilde{W}_A$ can be rewritten using Eq. (31) as

$$\tilde{W}_A(\xi)=G(\xi_0)\,\frac{(D^+(\xi)-D^-(\xi))}{(\xi-\xi_0)V(\xi)}, \tag{37}$$

where V is the dispersion function for a dry plate,

$$V(\xi)\equiv\frac{B}{\rho\omega^2}(\xi^4-\kappa^4), \tag{38}$$

and κ is the dry plate flexural wave number, defined by $\kappa^4=\omega^2 m/B$. The four zeros of $V(\xi)$ are evenly divided between $\mathscr{H}^+$ and $\mathscr{H}^-$, with the former pair being $\zeta_1=\kappa$ and $\zeta_2=i\kappa$. By adding and subtracting poles with suitable residues in Eq. (37) we can arrive at explicit formulae for the partitioned functions. For our purposes we need only

$$\begin{aligned}\tilde{W}_A^-(\xi)=\frac{G_A(\xi_0)}{\xi-\xi_0}\Bigg\{&\frac{D^+(\xi_0)}{V(\xi_0)}-\frac{D^-(\xi)}{V(\xi)}\\&+\sum_{n=1}^{2}\Bigg[\frac{(\xi-\xi_0)u_n^+}{(\xi-\zeta_n)(\zeta_n-\xi_0)}\\&+\frac{(\xi-\xi_0)u_n^-}{(\xi+\zeta_n)(-\zeta_n-\xi_0)}\Bigg]\Bigg\},\end{aligned} \tag{39}$$

where

$$u_n^\pm=\text{residue of}[D^\pm(\xi)/V(\xi)] \quad \text{at} \quad \xi=\pm\zeta_n. \tag{40}$$

The residues u_n^+ and u_n^- are related to one another by the fact that $D(\pm\zeta_n)=1$. Thus

$$u_n^\pm=\pm\frac{\zeta_n\rho}{4m}e^{\pm\nu_n}, \quad n=1,2, \tag{41}$$

where ν_1 and ν_2 are defined by

$$D^+(\zeta_n)=e^{\nu_n}, \quad n=1,2. \tag{42}$$

Suppose that $\tilde{W}_A^-(\xi)$ has the limiting behavior

$$\tilde{W}_A^-(\xi)=\sum_{n=0}^{M-1}\lambda_n\xi^{-(n+1)}+O(\xi^{-(M+1)}\log\xi),\quad |\xi|\to\infty, \tag{43}$$

for some integer $M\geqslant 1$, then

$$W_A(x)=\sum_{n=0}^{M-1}\lambda_n\frac{(ix)^n}{n!}+O(x^M\log x), \quad x\to+0. \tag{44}$$

According to its definition, $D^-(\xi)=O(\xi^{-5/2})$ as $|\xi|\to\infty$, and hence the first few λ_n can be obtained directly by expanding Eq. (39), yielding

$$\lambda_n=G_A(\xi_0)\Bigg\{\frac{D^+(\xi_0)}{V(\xi_0)}(\xi_0)^n+\sum_{m=1}^{2}\Bigg[\frac{u_m^+}{\zeta_m-\xi_0}-\frac{(-1)^n u_m^-}{\zeta_m+\xi_0}\Bigg](\zeta_m)^n\Bigg\}, \tag{45}$$

for $n=0,\ldots,5$.

We are now ready to apply the conditions of Eq. (13), using Eqs. (34a), (44), and (45). Assuming the polynomial expansion

$$A_A(\xi)=A_A^{(0)}+(A_1+A_2\xi)(\xi-\xi_0), \tag{46}$$

it follows after some algebra that the end conditions reduce to the system

$$\begin{bmatrix}\lambda_3-\xi_0\lambda_2 & \lambda_4-\xi_0\lambda_3\\ \lambda_4-\xi_0\lambda_3 & \lambda_5-\xi_0\lambda_4\end{bmatrix}\begin{bmatrix}A_1\\A_2\end{bmatrix}=\begin{bmatrix}\xi_0^2 p_{A,y}^{(0)}(0,0)-A_A^{(0)}\lambda_2\\ \xi_0^3 p_{A,y}^{(0)}(0,0)-A_A^{(0)}\lambda_3\end{bmatrix}. \tag{47}$$

This can be further reduced using the results of Eqs. (41), (45), and the identity

$$G_A(\xi_0)D^+(\xi_0)/V(\xi_0)=p_{A,y}^{(0)}(0,0)/A_A^{(0)}, \tag{48}$$

to give

$$(\mathbf{M}_1+\mathbf{M}_2)\begin{bmatrix}A_2\\A_1\end{bmatrix}=A_A^{(0)}\left(\frac{\mathbf{M}_1}{\xi_0^2-\zeta_1^2}+\frac{\mathbf{M}_2}{\xi_0^2-\zeta_2^2}\right)\begin{bmatrix}1\\\xi_0\end{bmatrix}, \tag{49}$$

where

$$\mathbf{M}_n=\begin{bmatrix}\cosh\nu_n & \zeta_n^{-1}\sinh\nu_n\\ \zeta_n\sinh\nu_n & \cosh\nu_n\end{bmatrix}, \quad n=1,2. \tag{50}$$

The pair of equations (49) are easily solved and combined with Eq. (46) to give, finally,

$$\begin{aligned}A_A(\xi)=\frac{A_A^{(0)}}{\xi_0^4-\kappa^4}\Bigg\{&\xi^2\xi_0^2-\kappa^4+\frac{(\xi-\xi_0)}{(\cosh\nu_1\cosh\nu_2+1)}\\&\times[(\xi-\xi_0)\zeta_1\zeta_2\sinh\nu_1\sinh\nu_2\\&+(\xi\xi_0+\zeta_1^2)\zeta_1\sinh\nu_1\cosh\nu_2\\&+(\xi\xi_0+\zeta_2^2)\zeta_2\sinh\nu_2\cosh\nu_1]\Bigg\}.\end{aligned} \tag{51}$$

III. THE ACOUSTIC DIFFRACTION COEFFICIENT

A. The exact diffraction coefficient

The symmetric and antisymmetric partial solutions may now be combined to give the total solution for the incident plane wave of Eq. (6),

$$p(x,y)=p^{(0)}(x,y)+p^{(1)}(x,y), \tag{52}$$

where the scattered response is

$$p^{(1)}(x,y)=\frac{1}{2\pi}\int_{-\infty}^{\infty}\tilde{p}(\xi,\xi_0)e^{(i\xi x-\gamma(\xi)|y|)}\,d\xi,\quad -\infty<x,\ y<\infty. \tag{53}$$

The transform $\tilde{p}=\tilde{p}_S+\tilde{p}_A$ follows from Eqs. (21), (28), (28), (30), and (51). This may be simplified further using Eqs. (22), (31), (A1), and (A2), to

$$\tilde{p}(\xi,\xi_0)=\frac{ip_0}{\xi-\xi_0}\frac{\gamma(\xi_0)}{D^+(\xi_0)D^+(-\xi)}\left[\gamma^-(\xi_0)\gamma^-(-\xi)+aF\left(\frac{\xi_0}{\kappa},-\frac{\xi}{\kappa}\right)\mathrm{sgn}(y)\right], \tag{54}$$

where the characteristic length a is defined by

$$a=m/\rho, \tag{55}$$

and

$$F(\zeta,\eta)=1-\zeta^2\eta^2+[(1-\zeta\eta)\sinh\nu_1\cosh\nu_2-i(1+\zeta\eta)\sinh\nu_2\cosh\nu_1-i(\zeta+\eta)\times\sinh\nu_1\sinh\nu_2]\frac{(\zeta+\eta)}{(1+\cosh\nu_1\cosh\nu_2)}. \tag{56}$$

The far-field diffracted pressure in the fluid may be found using the method of steepest descents applied to the integral in Eq. (53), and is a cylindrical wave emanating from the origin of the form

$$p^{(1)}=C(\theta,\theta_0)p_0\sqrt{2/(\pi kr)}e^{i\pi/4}e^{ikr},\quad r\rightarrow\infty,\quad 0<\theta\leq 2\pi. \tag{57}$$

The polar coordinates (r,θ) are defined in Fig. 2, and the dimensionless diffraction coefficient is

$$C(\theta,\theta_0)=-\frac{i}{2}k|\sin\theta|\tilde{p}(k\cos\theta,\quad k\cos\theta_0). \tag{58}$$

This can be simplified to

$$C(\theta,\theta_0)=\frac{\sin(\theta/2)\cos(\theta_0/2)-(i/2)kaF((k/\kappa)\cos\theta_0,-(k/\kappa)\cos\theta)\sin\theta\sin\theta_0}{(\cos\theta-\cos\theta_0)D^+(k\cos\theta_0)D^+(-k\cos\theta)}. \tag{59}$$

Equation (59) is valid for all $0\leq\theta_0\leq\pi$, $0\leq\theta\leq 2\pi$, except near the geometrical singularities at which $\cos\theta=\cos\theta_0$, corresponding to shadow and reflection boundaries. It is possible, although we will not do so here, to derive a uniform far-field approximation which is valid in these transition zones. We note that the diffraction coefficient of Eq. (59) clearly satisfies the reciprocity identity that it should be unaltered if the incident and scattering directions are interchanged, or

$$C(\theta,\theta_0)=\begin{cases}C(\pi-\theta_0,\pi-\theta), & 0\leq\theta\leq\pi,\\ C(\pi+\theta_0,\theta-\pi), & \pi\leq\theta\leq 2\pi.\end{cases} \tag{60}$$

B. Acoustic diffraction from a single plate

The acoustic diffraction coefficient for a single plate in a fluid can be obtained from the diffraction coefficient for a pair of plates. As discussed earlier, the single plate has bending stiffness $B'=2B$ and mass density $m'=2m$, and therefore the flexural wave number is the same, $\kappa'=\kappa$. The single plate diffraction coefficient is then the antisymmetric part of $C(\theta,\theta_0)$ for the pair of plates each with bending stiffness B and mass density m, or using Eq. (59),

$$C_{\mathrm{single}}(\theta,\theta_0)=\tfrac{1}{2}(C(\theta,\theta_0)-C(2\pi-\theta,\theta_0))=\frac{-ikaF((k/\kappa)\cos\theta_0,-(k/\kappa)\cos\theta)\sin\theta\sin\theta_0}{2(\cos\theta-\cos\theta_0)D^+(k\cos\theta_0)D^+(-k\cos\theta)},\quad \text{single plate}. \tag{61}$$

C. Discussion

1. Reference structures and characteristic frequencies

It is of interest to compare the exact acoustic diffraction coefficient of Eq. (59) with the analogous quantity for simpler diffracting structures. The two natural points of reference are the limiting cases of (i) an ideal hard screen in the same position as the plates, and (ii) a "soft" screen, for which the total pressure vanishes on the half-line $0<x<\infty$, $y=0$. Both of these are standard, canonical problems for which the diffraction coefficients can be obtained from Sommerfeld's classic solution as[15]

$$C_{\mathrm{hard}}(\theta,\theta_0)=\frac{\cos(\theta/2)\sin(\theta_0/2)}{\cos\theta-\cos\theta_0}, \tag{62a}$$

$$C_{\mathrm{soft}}(\theta,\theta_0)=\frac{\sin(\theta/2)\cos(\theta_0/2)}{\cos\theta-\cos\theta_0}. \tag{62b}$$

One immediate difference between both of these and the exact coefficient in Eq. (59) is that the latter depends upon the operating frequency, whereas C_{hard} and C_{soft} are constants. In order to discuss the frequency dependence we use a dimensionless measure of frequency, such as $ka=\omega/\omega_n$, where a is defined in Eq. (55) and $\omega_n\equiv\rho c/m$ is the "null" frequency at which $ka=1$. Alternatively, it is more common in fluid loaded structural acoustics problems involving flexural waves to use the dimensionless parameter $\Omega=k^2/\kappa^2$ or $\Omega=\omega/\omega_c$, where $\omega_c=c^2\sqrt{m/B}$ is the coincidence frequency for acoustic and flexural waves. The two parameters are related by

$$\Omega = \epsilon ka, \tag{63}$$

where $\epsilon = \omega_n/\omega_c$ is independent of the plate thickness and hence provides a useful measure of the fluid loading.

2. Low-frequency/heavy fluid-loading regime

We first consider the low-frequency limit, $\Omega \ll 1$. It may be shown using known expressions[16] for the limiting behavior of $D^+(\xi)$ that the terms $D^+(k\cos\theta_0)$, $D^+(-k\cos\theta)$, and F in Eq. (59) all tend to unity, and therefore,

$$C(\theta,\theta_0) \approx C_{\mathrm{soft}}(\theta,\theta_0) - i2ka\,\sin\frac{\theta}{2}\cos\frac{\theta_0}{2}\,C_{\mathrm{hard}}(\theta,\theta_0)$$

$$\to C_{\mathrm{soft}}(\theta,\theta_0) \quad \text{as} \quad \Omega \to 0. \tag{64}$$

This limiting behavior is not unexpected if one considers that at very low frequency, or equivalently, under heavy fluid-loading conditions, the inertial effects of the plate are negligible. Also, the geometry of the double plate structure exhibits no effective stiffness in the static limit. It is interesting to contrast this behavior with that of an empty cylindrical (in 2D) or spherical (in 3D) shell, which also show no inertial effects in this limit, but do display a finite stiffness in the static limit. Also, the leading order approximation to the diffraction from a single plate in the low-frequency limit follows from Eq. (61) as

$$C_{\mathrm{single}}(\theta,\theta_0) \approx \frac{-ika\,\sin\theta\,\sin\theta_0}{2(\cos\theta - \cos\theta_0)} \quad \text{as} \quad \Omega \to 0. \tag{65}$$

This tends to zero as $\omega \to 0$, in contrast to the exact diffraction coefficient which tends to a nonzero limit, in Eq. (64).

3. Light fluid-loading regime

The impedance length $a = m/\rho$ becomes large under light fluid-loading conditions, and we may accordingly approximate the dispersion function as $D = -\gamma V$. This is easily factorized to give

$$D^+(\xi) = a^{1/2}\kappa^{-2}\gamma^+(\xi)(\kappa+\xi)(\kappa - i\xi), \tag{66}$$

implying that

$$\begin{aligned} e^{\nu_1} &= -i(8ka)^{1/2}(1+\Omega^{-1/2})^{1/2}, \\ e^{\nu_2} &= (8ka)^{1/2}(i+\Omega^{-1/2})^{1/2}. \end{aligned} \tag{67}$$

Both of e^{ν_1} and e^{ν_2} are large in magnitude because $ka \gg 1$ by assumption, and therefore we may consistently take the approximations $\sinh\nu_n \to (1/2)e^{\nu_n}$, $\cosh\nu_n \to (1/2)e^{\nu_n}$, $n=1,2$, which imply that

$$D^+(k\cos\theta_0)D^+(-k\cos\theta)$$

$$= -i2ka\,\cos\frac{\theta_0}{2}\sin\frac{\theta}{2}\,F\left(\frac{k}{\kappa}\cos\theta_0, -\frac{k}{\kappa}\cos\theta\right). \tag{68}$$

The acoustic diffraction coefficient of Eq. (59) then becomes relatively simple in form,

$$C(\theta,\theta_0) = C_{\mathrm{hard}}(\theta,\theta_0), \tag{69}$$

to leading order in $(ka)^{-1}$ for $ka \gg 1$.

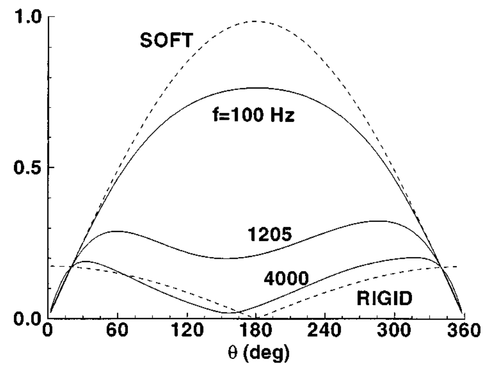

FIG. 3. The magnitude of the normalized exact diffraction coefficient $(\cos\theta - \cos\theta_0)C(\theta,\theta_0)$. The three solid curves are for the incident angle $\theta_0 = 20°$ and the frequencies 100, 1205, and 4000 Hz. The top and bottom dashed curves show the magnitudes of the frequency independent soft and hard normalized diffraction coefficients.

4. Example: steel plates in water

Numerical computations were performed for a steel/water combination, for which the fluid-loading parameter is $\epsilon = 0.134$. The thickness of each plate is 2.54 cm, corresponding to a null frequency of 1205 Hz and a coincidence frequency 8986 Hz. Figures 3 and 4 show the magnitude of the exact diffraction coefficient as a function of the observation angle θ for different frequencies. Note that the diffraction coefficient is multiplied by the factor $|\cos\theta - \cos\theta_0|$ in Fig. 3 and 4 in order to avoid the geometrical singularities at the reflection and shadow boundaries. The soft and hard diffraction coefficients are shown for comparison. The three frequencies considered, 100, 1205, and 4000 Hz, are low, medium, and high relative to the null frequency, and the high frequency is below coincidence. It is evident in both Figs. 3 and 4 that the low-frequency diffraction is more like that of a soft screen than a hard screen, but at high frequencies it is better approximated by the hard screen behavior. The same trend is apparent in Fig. 5 which shows the magnitude of the diffraction coefficient for backscatter, that is, $\theta = \theta_0 + \pi$.

Figure 6 shows the real and imaginary parts of the diffraction coefficient as a function of frequency for backscattering with $\theta_0 = 45°$. The transition from the soft response at low frequency to the high-frequency behavior is complicated by a change in the phase of the diffraction coefficient. In this particular case the soft and hard diffraction coeffi-

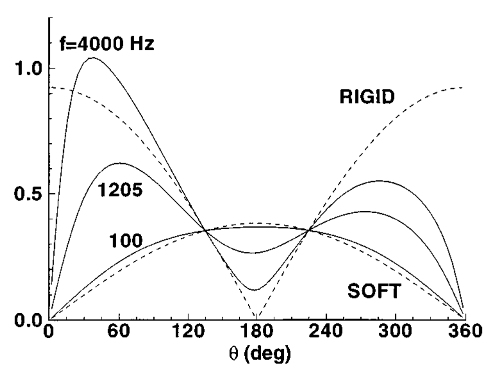

FIG. 4. The same as in Fig. 3 but for the incident angle 135°.

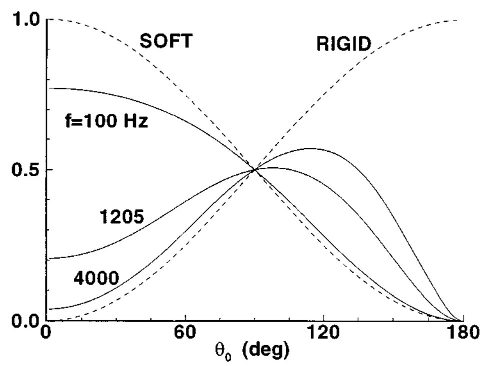

FIG. 5. The magnitude of the normalized backscattering diffraction coefficient, $-2 \cos \theta_0 C(\theta_0+\pi,\theta_0)$, for three frequencies.

cients are of opposite sign, or 180° different in phase. The frequency dependence of the phase of the exact diffraction coefficient is plotted in Fig. 7(b). The phase changes smoothly with frequency, although the total phase change is less than 180° over the frequency range considered.

In an attempt to better approximate the full frequency dependence of the diffraction we introduce the idea of an *intermediate frequency regime* defined such that the light fluid-loading condition $ka \gg 1$ holds while the frequency is low relative to the coincidence frequency, implying that $\Omega \ll 1$. This is an intermediate asymptotic situation which can only exist if the fluid-loading parameter ϵ is truly small. If so, then the frequency is both large and small at the same time, with respect to two different reference frequencies: in this case, $\omega_n \ll \omega \ll \omega_c$. Under these circumstances $F \approx 1$ in Eq. (59), and the acoustic diffraction coefficient is approximated by

$$C(\theta,\theta_0) \approx C_{\mathrm{hard}}(\theta,\theta_0) + \left(-i2ka \sin\frac{\theta}{2} \cos\frac{\theta_0}{2}\right)^{-1} C_{\mathrm{soft}}(\theta,\theta_0), \tag{70}$$

which is the same as Eq. (69) plus a correction of order $(ka)^{-1}$. Comparing Eqs. (64) and (70) suggests the following form for an approximation over the whole frequency range, $C \approx C_{\mathrm{unif}}$, where

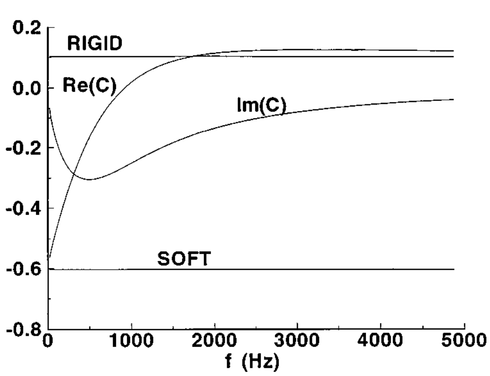

FIG. 6. The real and imaginary parts of the diffraction coefficient $C(\theta,\theta_0)$ for $\theta=225°$ and $\theta_0=45°$.

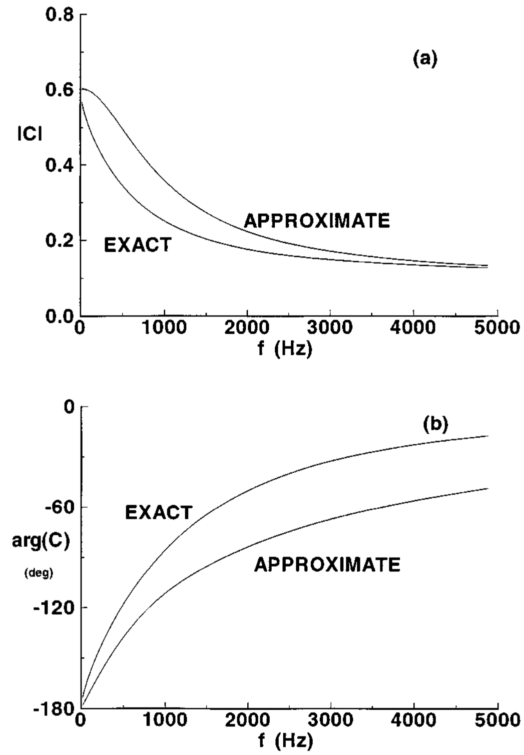

FIG. 7. Comparison of the exact diffraction with the approximate diffraction coefficient of Eq. (71) for the backscattering configuration $\theta=225°$ and $\theta_0=45°$. The magnitudes are plotted in (a), and the phase, or argument of the coefficients are shown in (b).

$$\begin{aligned} C_{\mathrm{unif}}(\theta,\theta_0) &\equiv \frac{C_{\mathrm{soft}}(\theta,\theta_0) - i2ka \sin(\theta/2)\cos(\theta_0/2) C_{\mathrm{hard}}(\theta,\theta_0)}{1 - i2ka \sin(\theta/2)\cos(\theta_0/2)} \\ &= C_{\mathrm{soft}}(\theta,\theta_0)\left(\frac{1 - i2ka \sin(\theta_0/2)\cos(\theta/2)}{1 - i2ka \sin(\theta/2)\cos(\theta_0/2)}\right). \end{aligned} \tag{71}$$

This function has the property of reducing to the limiting soft and hard approximate forms at low frequency and under light fluid-loading conditions, respectively. The latter situation is synonymous with high frequency in the sense of $ka \gg 1$ if $\epsilon \ll 1$. It should be emphasized that Eq. (71) is not a uniform approximation in the usual sense. Rather, it is simply an educated guess at such an approximation which has the useful features of (i) being composed of the well-known soft and hard diffraction coefficients, (ii) it reproduces the limiting soft and hard behavior discussed above, and (iii) is defined for all frequencies. We make no claims about the universal accuracy of this approximation, but offer it as a useful benchmark for acoustic diffraction from wave-bearing structures. For example, the magnitude and phase of the exact and "uniform" diffraction coefficients are compared in Fig. 7(a) and (b) for the backscattering configuration of Fig. 6.

Finally, we note that the most common scattering configuration is backscatter ($\theta=\theta_0+\pi$). In this case, it can be shown using Eqs. (62a) and (62b) that the soft and hard diffraction coefficients are always of opposite sign. Hence, the exact backscatter diffraction coefficient will exhibit an approximately 180° phase change as the frequency is swept from low to high. This can have interesting implications for the time-dependent edge diffraction, which will be explored elsewhere.

IV. CONCLUSION

The exact acoustic diffraction coefficient derived here for the parallel double plate configuration, Eq. (59), is relatively explicit in form and reduces to the simpler soft and hard diffraction coefficients in certain limits. The general solution also contains the solution for the acoustic diffraction from a single semi-infinite thin plate in a fluid. The numerical computation of the exact diffraction coefficient of Eq. (59) requires the function D^+ of the Appendix, which is easily evaluated in practice. However, the analytical form of Eq. (59) is sufficiently explicit and simple in nature that it can be easily reduced to the limiting cases of soft and hard diffraction coefficients under heavy fluid and light fluid-loading conditions, respectively. The former limit means that the low-frequency limit of the diffraction coefficient is particularly simple, and in contrast to the low-frequency limit for a single plate in a fluid, the double plate coefficient has a finite value as $\omega \to 0$. Most significantly, the analytical relationships that we have established here linking the exact solution with the soft and hard screen limits allows us to use these limits under identifiable circumstances. Thus the soft screen approximation is valid at low frequency, while the hard screen is a better approximation at higher frequencies. The transition is defined by the null frequency $\omega_n \equiv \rho c/m$. The diffraction coefficient cannot be so simply approximated for frequencies close to ω_n, although we have suggested a qualitative approximation in Eq. (71).

ACKNOWLEDGMENT

This work was supported by the Office of Naval Research.

APPENDIX: FACTORIZATION OF THE KERNEL

The Wiener–Hopf factors of $\gamma(\xi)$ are defined as such that $\gamma = \gamma^+/\gamma^-$ and $\gamma^-(-\xi) = 1/\gamma^+(\xi)$, or explicitly,

$$\gamma^{\pm}(\xi) = e^{\mp i\pi/4}(k \pm \xi)^{\pm 1/2}. \tag{A1}$$

The factors of K defined in Eqs. (19) and (20) are therefore

$$K^{\pm}(\xi) = D^{\pm}(\xi)/\gamma^{\pm}(\xi). \tag{A2}$$

The functions $D^{\pm}$ have been derived previously in several different forms.[7,16] Recently, a new and easily computable expression was derived by Norris and Wickham,[11] which we summarize here. Thus the ten zeros of the rationalized function $1-\gamma^2(\xi)V^2(\xi)$ are $\pm\xi_n$, $n=1,2,\ldots,5$, defined such that ξ_n are in $\mathscr{H}^+$. Of these five, it can be shown that three, say ξ_1, ξ_3, and ξ_5, are zeros of $D(\xi)$. Define $\theta_n = \cos^{-1}(\xi_n/k)$, $n=1,2,\ldots,5$, where the branch of the inverse cosine is $\cos^{-1}(\xi/k) = i \log[\xi/k + \gamma(\xi)/k]$, and the principal branch of the logarithm is taken, $-\pi < \mathrm{Im}\log(\cdot) < \pi$. Then

$$\begin{aligned} D^+(\xi) = {} & (1-ika)^{1/2}\left(1+\frac{\xi}{\xi_1}\right)\left(1+\frac{\xi}{\xi_3}\right)\left(1+\frac{\xi}{\xi_5}\right) \\ & \times \exp\left\{\frac{1}{2\pi}\int_{\pi/2}^{\cos^{-1}\xi/k}\sum_{n=1}^{5}\left[\frac{\theta \sin\theta_n - \theta_n \sin\theta}{\cos\theta - \cos\theta_n}\right.\right. \\ & \left.\left. + \frac{\theta\sin\theta_n - (\pi-\theta_n)\sin\theta}{\cos\theta + \cos\theta_n}\right](-1)^n d\theta\right\}, \end{aligned} \tag{A3}$$

where a is defined in Eq. (55). The function D^- then follows from Eqs. (31) and (A3).

[1] J. B. Keller, ‘‘Diffraction by an aperture,’’ J. Appl. Phys. **28**, 426–444 (1957).
[2] D. G. Crighton, ‘‘The 1988 Rayleigh medal lecture: Fluid loading—the interaction between sound and vibration,’’ J. Sound Vib. **133**, 1–27 (1989).
[3] G. L. Lamb, ‘‘Diffraction of a plane sound wave by a semi-infinite thin elastic plate,’’ J. Acoust. Soc. Am. **31**, 929–935 (1959).
[4] L. M. Lyamshev, ‘‘Sound diffraction by a semi-infinite elastic plate in a moving medium,’’ Sov. Phys. Acoust. **12**, 291–294 (1967).
[5] D. G. Crighton, ‘‘Acoustic edge scattering of elastic surface waves,’’ J. Sound Vib. **22**, 25–32 (1972).
[6] P. A. Cannell, ‘‘Edge scattering of aerodynamic sound by a lightly loaded elastic half-plane,’’ Proc. R. Soc. London Ser. A **347**, 213–238 (1975).
[7] P. A. Cannell, ‘‘Acoustic edge scattering by a heavily loaded elastic half-plane,’’ Proc. R. Soc. London Ser. A **350**, 71–89 (1976).
[8] D. P. Kouzov, ‘‘Diffraction of a plane hydroacoustic wave on the boundary of two elastic plates,’’ Prikl. Mat. Mekh. **27**, 541–546 (1963).
[9] P. R. Brazier-Smith, ‘‘The acoustic properties of two co-planar half-plane plates,’’ Proc. R. Soc. London Ser. A **409**, 115–139 (1987).
[10] S. Asghar, A. Hussain, and B. Ahmad, ‘‘The scattering of an acoustic wave from the absorbing-elastic coupling of two half-planes,’’ J. Acoust. Soc. Am. **95**, 34–39 (1994).
[11] A. N. Norris and G. R. Wickham, ‘‘Acoustic diffraction from the junction of two flat plates,’’ Proc. R. Soc. London **451**, 631–656 (1995).
[12] A. N. Norris and D. A. Rebinsky, ‘‘The line admittance at the junction of two plates with and without fluid loading,’’ J. Sound Vib. (in press).
[13] D. A. Rebinsky and A. N. Norris, ‘‘Acoustic and flexural wave scattering from a three member junction,’’ J. Acoust. Soc. Am. **98**, 3309–3319 (1995).
[14] There is an error in Eq. (4.11) of Cannell’s 1975 paper (Ref. 6). It should read $N(s) = \phi^0_{yxxx} - is\phi^0_{yxx} - s^2\phi^0_{yx} + is^3\phi^0_y$.
[15] B. Noble, *Methods Based on the Wiener–Hopf Technique* (Pergamon, New York, 1958).
[16] D. G. Crighton and D. Innes, ‘‘The modes, resonances and forced response of elastic structures under heavy fluid loading,’’ Philos. Trans. R. Soc. London Ser. A **312**, 295–341 (1984).